Applications and Applied Mathematics: An International Journal (AAM)

Volume 14 | Issue 1 Article 41

6-2019

Closed Form Solutions of Unsteady Two Fluid Flow in a Tube

J. Liu
Michigan State University

C. Y. Wang
Michigan State University

Available at
http://pvamu.edu/aam
Appl. Appl. Math.
ISSN: 1932-9466

Applications and Applied Mathematics:
An International Journal
(AAM)

Vol. 14, Issue 1 (June 2019), pp. 586 - 601

Closed-Form Solutions of Unsteady Two-Fluid Flow in a Tube

J. Liu and C.Y. Wang

Department of Mathematics
Michigan State University
East Lansing, MI 48824
E-mail: cywang@mth.msu.edu

Received: July 5, 2018; Accepted: September 27, 2018

Abstract

Exact closed-form solutions for the mathematical model of unsteady two-fluid flow in a circular tube are presented. The pressure gradient is assumed to be oscillatory or exponentially increasing or decreasing in time. The instantaneous velocity profiles and flow rates depend on the size of the core fluid, the density ratio, the viscosity ratio, and a parameter (e.g. the Womersley number) quantifying time changes. Applications include blood flow in small vessels.

Keywords: Exact solution; Viscous flow; Two-fluid; Unsteady; Blood flow

MSC 2010 No.: 76Z05, 76D50, 92C35

1. Introduction

Viscous flow in a tube is fundamental in fluid mechanics. In some cases the fluid is not homogeneous but can be well-modeled by two different immiscible homogeneous fluids, i.e., a core fluid and a boundary fluid. Practical examples include lubricated walls in food processing, micro-fluidic super-hydrophobic liquid flow due to a layer of trapped gas, and fluids with particulate suspensions, especially blood flow in small vessels.

The steady, two fluid layer *channel* flow, important in transport processes in chemical engineering, was solved by Bird et al. (2007). It was extended to starting flow by Wang (2017), exponentially increasing unsteady flow by Kapur and Shukla (1964), and oscillatory flow by Bhattacharyya (1968). The last two references considered the special case where the two fluid layers were of exactly the same thickness.

The steady concentric two-fluid *tube* flow was first proposed by Vand (1948) for the flow of ink suspension in tubes. Hayes (1960) and Sharan and Popel (2001) successfully applied the two-fluid model to blood flow in small vessels. Notable extensions include the application to stenotic vessels (Shukla et al. 1980), non-Newtonian core fluid (Srivastava and Saxena 1994), and curved vessels (Wang and Bassingthwaighte 2003). The model also describes the laminar transport of oil with a lubricating envelope of water (Martinez-Palou et al. 2011). There seems to be very few *unsteady* two-fluid flow solutions. Bugliarello and Sevilla (1970) formulated the pulsatile (oscillatory) flow problem but did not give the solution or any results. The purpose of the present paper is to present the (only two) unsteady closed-form solutions of two-fluid tube flow. These exact solutions also serve as benchmarks for approximate methods, such as numerical, series, or perturbation results. The properties of these solutions are important not only to the afore-mentioned engineering applications but also to blood flow in small vessels.

Modeling blood flow in the circulation primarily depends on the diameter of the blood vessel (relative to the size of the suspended red blood cells). It is generally accepted that for large blood vessels blood can be considered as a homogeneous fluid with a viscosity about 3-4 times that of water. If the vessel diameter is between 1-2 mm, blood could be modeled by a two-phase fluid where blood and plasma have separate dynamics (e.g., Chow 1975, Srivastava and Srivastava 1983). If the size of the blood vessel is less than 1000 microns (1 mm) and down to 40 microns, the apparent viscosity decreases. This phenomenon, or Fahraeus-Lindqvist effect, can be explained by the steric hindrance of the red blood cells near the wall, where a less viscous, relatively cell-free plasma layer exists (Pries et al. 1996). For this range of vessel diameters, it is natural to use the two-fluid model to describe blood flow. Wang and Bassingthwaighte (2003) successfully curve-fitted the the two-fluid theory with the experimental data of Pries (1996) and Secomb (1995) for various hematocrit contents. It is found that nonlinear effects such as shear dependence, rouleaux formation, wall deformation, cell deformation etc are contained in the curve fit. For vessel diameters less than 10 microns, the apparent viscosity increases due to the resistance of individual (now comparable in size) red blood cells. Thus the present work shall be applicable to blood flow in vessels of 40-1000 microns in diameter.

2. Formulation

First we formulate the generic unsteady axisymmetric two-fluid problem. Figure 1 shows a section of the long tube where region 1 is the core fluid and region 2 is the annular boundary fluid. The Navier-Stokes equation for parallel flow degenerates to

$$\frac{\partial u_1'}{\partial t'} = -\frac{1}{\rho_1}\frac{\partial p'}{\partial z'} + \frac{\nu_1}{r'}\frac{\partial}{\partial r'}\left(r'\frac{\partial u_1'}{\partial r'}\right), \tag{1}$$

$$\frac{\partial u_2'}{\partial t'} = -\frac{1}{\rho_2}\frac{\partial p'}{\partial z'} + \frac{\nu_2}{r'}\frac{\partial}{\partial r'}\left(r'\frac{\partial u_2'}{\partial r'}\right). \tag{2}$$

Here u' is axial velocity in the axial z' direction, t' is the time, p is the pressure, ρ is the density, ν is the kinematic viscosity, and r' is the radial coordinate. The primes mean dimensional quantities and the subscripts indicate the region. An unsteady pressure gradient of magnitude G_0 is applied.

$$\frac{dp'}{dz'} = -G_0 g(t') . \tag{3}$$

Normalizing all lengths by the tube radius a, the time by a^2/ν_1, the velocity by $a^2 G_0/(\rho_1 \nu_1)$ and dropping primes, equations (1) and (2) reduce to

$$u_{1t} = g + (r u_{1r})_r / r , \qquad 0 \le r \le \lambda , \tag{4}$$

$$u_{2t} = \gamma g + \beta^{-2} (r u_{2r})_r / r , \qquad \lambda \le r \le 1 . \tag{5}$$

Here, λ (<1) is the normalized core radius,

$$\gamma = \rho_1 / \rho_2 , \ \beta^2 = \nu_1 / \nu_2 , \tag{6}$$

are density and kinematic viscosity ratios. The boundary conditions are that the velocity is bounded on the axis, no slip on the wall and velocities and shear stresses match on the interface at $r = \lambda$:

$$u_1 = u_2 , \tag{7}$$

$$\gamma \beta^2 u_{1r} = u_{2r} . \tag{8}$$

We shall consider the two cases which yield closed-form solutions, that when the pressure gradient is oscillatory, and when the pressure gradient is exponential in time.

3. Oscillatory flow

For oscillatory flow, let

$$g = e^{i\omega t'} = e^{is^2 t} , \tag{9}$$

$$s = \sqrt{\omega a^2 / \nu_1} , \tag{10}$$

where ω is the dimensional frequency, $i = \sqrt{-1}$, s is the Womersley number, and only the real part of any physical term has significance. Let

$$u_1 = e^{is^2 t} f_1(r), \quad u_2 = e^{is^2 t} f_2(r) . \tag{11}$$

Equations (4) and (5) reduce to

$$f_1''+\frac{1}{r}f_1'-is^2 f_1=-1\ , \tag{12}$$

$$f_2''+\frac{1}{r}f_2'-is^2\beta^2 f_2=-\gamma\beta^2 . \tag{13}$$

The solutions satisfying boundedness on the axis and zero on the wall is

$$f_1=\frac{-i}{s^2}\left[1+C_1 J_0(ksr)\right], \tag{14}$$

$$f_2=\frac{-i\gamma}{s^2}\left[1+(C_2-1)\frac{J_0(ks\beta r)}{J_0(ks\beta)}-C_2\frac{Y_0(ks\beta r)}{Y_0(ks\beta)}\right]. \tag{15}$$

Here, $k=(i-1)/\sqrt{2}$, J_0 and Y_0 are Bessel functions of the first and second kind, and C_1, C_2 are constants to be determined by equations (7,8). We find

$$\begin{aligned}
C_1 &= \{J_1(ks\beta\lambda)[(\gamma-1)Y_0(ks\beta)-\gamma Y_0(ks\beta\lambda)] \\
&\quad -Y_1(ks\beta\lambda)[(\gamma-1)J_0(ks\beta)-\gamma J_0(ks\beta\lambda)]\}/\Delta_1, \\
C_2 &= \{[\beta(\gamma-1)J_0(ks\beta)J_1(ks\lambda)-\beta\gamma J_0(ks\beta\lambda)J_1(ks\lambda) \\
&\quad +J_0(ks\lambda)J_1(ks\beta\lambda)]Y_0(ks\beta)\}/\Delta_1, \\
\Delta_1 &= \beta\gamma J_1(ks\lambda)[J_0(ks\beta)Y_0(ks\beta\lambda)-Y_0(ks\beta)J_0(ks\beta\lambda)] \\
&\quad +J_0(ks\lambda)[Y_0(ks\beta)J_1(ks\beta\lambda)-J_0(ks\beta)Y_1(ks\beta\lambda)].
\end{aligned} \tag{16}$$

For a single fluid, one can set $\lambda=1$ or $\gamma=\beta=1$. The solution degenerates to

$$u=\frac{e^{is^2t}}{is^2}\left[1-\frac{J_0(ksr)}{J_0(ks)}\right]. \tag{17}$$

This is the solution of the oscillatory single-fluid flow in a circular tube found by Sexl (1930).

The steady-state solution of the two-fluid flow can be obtained by letting s = 0 and solving equations (12) and (13). We find the velocity profile is composed of two different paraboloids,

$$u_{10}=\frac{1}{4}[\gamma\beta^2(1-\lambda^2)+\lambda^2-r^2], \tag{18}$$

$$u_{20}=\frac{\gamma\beta^2}{4}(1-r^2). \tag{19}$$

This steady-state solution agrees with all previous reports. Although our equations (14) and (15) do not directly accept s = 0, the steady-state solution can be recovered by taking the analytic limit $s\to 0$, or evaluating numerically by letting s to be a small number,

such as $s = 0.0001$. The steady-state flow rate is

$$Q_0 = 2\pi\int_0^{\lambda} u_{10} r dr + 2\pi\int_{\lambda}^{1} u_{20} r dr = \frac{\pi}{8}[\lambda^4 + \beta^2\gamma(1-\lambda^4)]. \tag{20}$$

Note that for $\lambda = 1$, or for $\beta\gamma^2 = 1$, the two-fluid steady-state solution reduces to the well-known single-fluid Poiseuille solution.

Figure 2 shows some typical oscillatory velocity profiles. The velocity is composed of two parts, discontinuous in slope at the interface, and its magnitude is oscillatory. It is seen that at low Womersley number *s*, the velocity profile is similar to the steady-state case, with maximum on the axis of the tube. However, for *s* large, the maximum velocity moved closer to the walls. This phenomenon, called the "annular effect", also exists for single-fluid oscillatory flows (see e.g., Schlichting and Gersten 2000).

The instantaneous flow rate is

$$Q = 2\pi\int_0^{\lambda} u_1 r dr + 2\pi\int_{\lambda}^{1} u_2 r dr \equiv E_1\cos(s^2 t) - E_2\sin(s^2 t). \tag{21}$$

The amplitude *A* and the phase lag *P* of the flow rate are

$$A = \sqrt{E_1^2 + E_2^2} \quad \text{and} \quad P = \tan^{-1}(E_2 / E_1). \tag{22}$$

Figure 3 shows the amplitude decays from the steady state value to zero as frequency is increased. The effect of increased core diameter λ is to decrease the amplitude, while increased viscosity ratio β increases the amplitude. Figure 4 shows the phase of the oscillatory flow rate lags behind the oscillatory pressure. The phase lag is small for low frequencies, but increases to $\pi/2$ for large frequencies. Also shown are the effects of λ and β.

Also of interest is the shear stress on the wall. The shear stress, normalized by aG_0, is

$$\tau = \frac{1}{\gamma\beta^2}\frac{\partial u_2}{\partial r}(1,t). \tag{23}$$

The magnitude of the shear stress

$$M = \frac{|f_2'(1)|}{\gamma\beta^2}, \tag{24}$$

is plotted in Figure 5. We see that an increase in λ or a decrease in β increases the

shear stress. Increased shear stress retards accumulation of deposits, such as atherosclerosis in vascular vessels.

4. Exponential Acceleration or Deceleration

Another closed-form solution is possible when the unsteady pressure gradient is exponentially growing or decaying in time. Let $b > 0$ be a measure of the rate of increase or decrease

$$g = e^{\pm bt'} = e^{\pm \alpha^2 t}, \qquad \alpha = \sqrt{ba^2/\nu_1} \quad . \tag{25}$$

Here, the top sign is for increasing pressure gradient and the bottom sign is for decreasing pressure gradient. Let

$$u_1 = e^{\pm \alpha^2 t} h_1(r), \quad u_2 = e^{\pm \alpha^2 t} h_2(r). \tag{26}$$

Equations (4) and (5) reduce to

$$h_1'' + \frac{1}{r} h_1' \mu \alpha^2 h_1 = -1, \tag{27}$$

$$h_2'' + \frac{1}{r} h_2' \mu \alpha^2 \beta^2 h_2 = -\gamma \beta^2. \tag{28}$$

The solution for the case of increasing pressure gradient is

$$h_1 = \frac{1}{\alpha^2}\left[1 + B_1 I_0(\alpha r)\right], \tag{29}$$

$$h_2 = \frac{\gamma}{\alpha^2}\left[1 + (B_2 - 1)\frac{I_0(\alpha\beta r)}{I_0(\alpha\beta)} - B_2 \frac{K_0(\alpha\beta r)}{K_0(\alpha\beta)}\right]. \tag{30}$$

Here, I_0 and K_0 are modified Bessel functions. The matching conditions, then, determine the constants, i.e.,

$$\begin{aligned} B_1 &= \{I_1(\alpha\beta\lambda)[(\gamma-1)K_0(\alpha\beta) - \gamma K_0(\alpha\beta\lambda)] \\ &\quad + K_1(\alpha\beta\lambda)[(\gamma-1)I_0(\alpha\beta) - \gamma I_0(\alpha\beta\lambda)]\}/\Delta_2, \\ B_2 &= K_0(\alpha\beta)[(\gamma-1)\beta I_0(\alpha\beta) I_1(\alpha\lambda) \\ &\quad - \beta\gamma I_0(\alpha\beta\lambda) I_1(\alpha\lambda) + I_0(\alpha\lambda) I_1(\alpha\beta\lambda)]/\Delta_2, \\ \Delta_2 &= \beta\gamma I_1(\alpha\lambda)[I_0(\alpha\beta) K_0(\alpha\beta\lambda) - K_0(\alpha\beta) I_0(\alpha\beta\lambda)] \\ &\quad + I_0(\alpha\lambda)[I_0(\alpha\beta) K_1(\alpha\beta\lambda) + K_0(\alpha\beta) I_1(\alpha\beta\lambda)]. \end{aligned} \tag{31}$$

Figure 6 shows the velocity profiles, here normalized by the maximum velocity which occurs on the axis. When the acceleration parameter α is zero, the velocity profile is

that of the steady-state solution. As α increases, the velocity profile becomes more blunted. For different times, the velocity profiles are similar, i.e., as time increases the magnitudes increase exponentially. The instantaneous flow rate is

$$\begin{aligned} Q = e^{\alpha^2 t} 2\pi \{ & 2(B_2 - 1)\gamma K_0(\alpha\beta)[I_1(\alpha\beta) - \lambda I_1(\alpha\beta\lambda)] \\ & + 2B_2\gamma I_0(\alpha\beta)[K_1(\alpha\beta) - \lambda K_1(\alpha\beta\lambda)] \\ & + \beta I_0(\alpha\beta)K_0(\alpha\beta)[\alpha(\gamma + \lambda^2 - \gamma\lambda^2) \\ & - 2B_1\lambda I_1(\alpha\lambda)]\} / [2\beta\alpha^3 I_0(\alpha\beta)K_0(\alpha\beta)]. \end{aligned} \tag{32}$$

In the case of a *single* fluid with exponentially increasing pressure gradient, our solution reduces to

$$u = \frac{e^{\alpha^2 t}}{\alpha^2}\left[1 - \frac{I_0(\alpha r)}{I_0(\alpha)}\right]. \tag{33}$$

This exact solution agrees with that of Sanyal (1956).

For the exponentially decreasing pressure gradient, we find

$$h_1 = \frac{-1}{\alpha^2}\left[1 + D_1 J_0(\alpha r)\right], \tag{34}$$

$$h_2 = \frac{-\gamma}{\alpha^2}\left[1 + (D_2 - 1)\frac{J_0(\alpha\beta r)}{J_0(\alpha\beta)} - D_2\frac{Y_0(\alpha\beta r)}{Y_0(\alpha\beta)}\right], \tag{35}$$

$$\begin{aligned} D_1 &= \{J_1(\alpha\beta\lambda)[(\gamma - 1)Y_0(\alpha\beta) - \gamma Y_0(\alpha\beta\lambda)] \\ &\quad - Y_1(\alpha\beta\lambda)[(\gamma - 1)J_0(\alpha\beta) - \gamma J_0(\alpha\beta\lambda)]\} / \Delta_3, \\ D_2 &= Y_0(\alpha\beta)\{\beta J_1(\alpha\lambda)[(\gamma - 1)J_0(\alpha\beta) - \gamma J_0(\alpha\beta\lambda)] \\ &\quad + J_0(\alpha\lambda)J_1(\alpha\beta\lambda)\} / \Delta_3, \\ \Delta_3 &= \beta\gamma J_1(\alpha\lambda)[J_0(\alpha\beta)Y_0(\alpha\beta\lambda) - Y_0(\alpha\beta)J_0(\alpha\beta\lambda)] \\ &\quad + J_0(\alpha\lambda)[Y_0(\alpha\beta)J_1(\alpha\beta\lambda) - J_0(\alpha\beta)Y_1(\alpha\beta\lambda)]. \end{aligned} \tag{36}$$

In the case of a single fluid, put $\lambda = 1$ or $\beta = \gamma = 1$, and the solution becomes

$$u = e^{-\alpha^2 t}h(r), \qquad h = \frac{-1}{\alpha^2}\left[1 - \frac{J_0(\alpha r)}{J_0(\alpha)}\right]. \tag{37}$$

Equation (37) reduces to the paraboloidal Poiseuille velocity when α =0. However, it fails when α is increased to 2.4048, or the first zero of J_0. This is because the velocity can no longer be described by the same exponential decay as the pressure gradient. The solution should be replaced by

$$u = \frac{e^{-\alpha^2 t}}{\alpha^2 G(1)}\left[tJ_0(\alpha r) + G(r) - G(1) + c_1 J_0(\alpha r)\right], \tag{38}$$

$$G(r) = \frac{\pi r^2}{4} J_1(\alpha r)\left[J_1(\alpha r)Y_0(\alpha r) - J_0(\alpha r)Y_1(\alpha r)\right]. \tag{39}$$

Note that there is a homogeneous solution with arbitrary constant c_1 which depends on the initial conditions, and the existence of a slower decay $te^{-\alpha^2 t}$ term. We shall limit equation (37) to $0 < \alpha < 2.4048$, since for large α values the pressure decrease is too precipitous to be practical. For example, experimental measurements after the occlusion of 100 micron microvessels show the pressure decreased with two slowly decaying exponentials of $\alpha = 0.028$ and 0.079, (Maarek et al. 1990).

For two-fluid flow, the exact solution equations (26), (34) and (35) is also limited in the deceleration rate. The upper limit range for the exponent α is found from the zero of the denominator of the coefficient D_1 given in Table 1.

Table 1. Upper limit for deceleration exponent α for the case $\gamma = 1$

$\lambda \backslash \beta$	1	1.5	2	2.5	3
0.8	2.4048	1.9305	1.5615	1.2953	1.1011
0.85	2.4048	2.0108	1.6802	1.4159	1.2148
0.9	2.4048	2.1287	1.8450	1.5966	1.3930
0.95	2.4048	2.2586	2.0800	1.8923	1.7133
1	2.4048	2.4048	2.4048	2.4048	2.4048

The decelerating velocity profiles for the admissible α ranges are similar to the steady-state profiles and are not presented here. The instantaneous flow rate is

$$\begin{aligned} Q = e^{-\alpha^2 t} 2\pi \{ & 2(1-D_2)\gamma Y_0(\alpha\beta)[J_1(\alpha\beta) - \lambda J_1(\alpha\beta\lambda)] \\ & + 2D_2\gamma J_0(\alpha\beta)[Y_1(\alpha\beta) - \lambda Y_1(\alpha\beta\lambda)] \\ & + \beta J_0(\alpha\beta)Y_0(\alpha\beta)[\alpha(\gamma\lambda^2 - \gamma - \lambda^2) \\ & - 2D_1\lambda J_1(\alpha\lambda)]\} / [2\beta\alpha^3 J_0(\alpha\beta)Y_0(\alpha\beta)]. \end{aligned} \tag{40}$$

5. Discussion

Axisymmetric two-fluid flow in a tube is also called core-annular flow, important in the transport of viscous liquids such as oil. The *steady* core-annular flow has been studied by many authors, both theoretically (for stability) and experimentally. The existence of a stable core-annular flow depends on the inner diameter of the tube, the diameter of the core fluid, the densities, viscosities and velocities of the two fluids, the material and smoothness of the wall, the orientation with respect to gravity, and whether surfactants are added. See the review of Ghosh et al. (2009) for the details.

We are interested in the two-fluid tube flow and its applications to blood flow. As mentioned before, experimental blood flow properties such as velocity and resistance (including the Fahraeus-Lindqvist effect) in the microvasculature can be predicted by the two-fluid model. The parameter ranges for which the two-fluid model is applicable are as follows: the (inner) vessel diameter between 40-1000 microns, the hematocrit between 15% to 60%, the ratio of the core diameter to the vessel diameter between 0.82 to 1, and the ratio of core viscosity to plasma viscosity between 1.5 to 5. See Wang and Bassingthwaighte (2003) and Wang (2008) for the justification of using the two-fluid model in explaining the experimental results.

The pressure gradient of our analysis is assumed to be either sinusoidal or exponential in time. In practice the pressure gradient may be pulsatile, which can be decomposed into a steady part and an oscillatory part. The oscillatory part may be further Fourier decomposed to a sum of single harmonics. For example, we found a typical pressure measurement in a venule (e.g., Gaehtgens 1970) can be very accurately represented by a constant and several sinusoidal harmonics, each with its own amplitude and phase.

Aside from geometric factors, oscillatory flow is governed by the Womersley number s in equation (10). For normal blood flow in arterioles of 100 micron diameter, and a resting frequency of 60 beats per minute, we find the (dominant harmonic) s is about 0.1. The value of s is about 1 for birds with a heart beat of 900 beats per minute. The s value for the higher harmonics may be several times larger.

The exponentially growing or exponentially decaying solutions model increased or decreased pressure gradient as in opening or closing a valve or a sphincter. These results are quite different from those of the oscillatory flow. These exponential solutions can also be superposed. For example, it was found that micro-vascular pressure measurements decays after an arterial occlusion. This pressure decay can be described by the sum of two exponentials (Pellett et al. 1999). Then using our analysis, the velocity, flow and stress properties (which are difficult to measure) can be predicted.

In order to maintain the interface between the two fluids, gravity effects must not be important, or the density ratio γ is close to one. This is indeed true for suspensions such as ink or blood. To illustrate, it takes much effort by ultracentrifuge to separate plasma from whole blood. Thus in normal circumstances the interface is maintained.

Our exact solutions may be limited by stability. Using a perturbation on the exact solutions found in this paper, the resulting Orr-Sommerfeld equation can be analyzed using Floquet theory (for oscillatory flow) and/or numerical integration. This has not been done due to the limited aims of the present paper. However, some conclusions about stability can be made from existing reports as follows.

Oscillatory tube flow is governed by an oscillatory Reynolds number defined as

$$\mathrm{Re} = \frac{U}{\sqrt{2\nu\omega}}, \tag{41}$$

where U is the maximum oscillatory velocity. Typical experimental observations in a cat venule of 78 micron diameter yield a maximum velocity about 10.67 ± 0.33 cm/sec at a frequency of 2.5 beats/sec (Intaglietta et al. 1971). Using these values we find Re=0.37 from Equation (41). The steady through-flow Reynolds number is also small, about 3.34.

Thomas et al. (2011) used linear stability theory on single-fluid oscillatory tube flow. They found the critical oscillatory Reynolds number to be 600-700, which is two or three times the experimentally measured values. The addition of a steady through flow increased stability. For two-fluid tube flow, there are added stability concerns at the interface due to differences in density, velocity and shear, aside from surface tension. Using linear analysis, Preziosi et al. (1989) predicted the two-fluid steady tube flow is stable for Reynolds numbers below about 100. At small Reynolds numbers the flow may be unstable to long waves due to surface tension. However, surface tension is absent for our two-fluid blood flow model, since the interface is due to steric hindrance instead of a true immiscible interface. Since both oscillatory and through-flow Reynolds numbers are of order unity (even for larger micro-vessels), we can safely conclude oscillatory (and pulsatile) two-fluid blood flow in micro-vessels are stable.

6. Conclusions

Exact closed-form solutions of the Navier-Stokes equations are found for the unsteady two-fluid motion in a tube.

An important parameter governing oscillatory flow is the Womersley number *s*. At small *s* the velocity profile is composed of two paraboloids, with a kink at the interface. At large *s* the velocity profile exhibits "annular effect", or its maximum moves toward the wall. For a given oscillatory pressure, the flow rate decreases with larger *s*, larger core radius fraction, and smaller viscosity ratio.

The velocity profile for exponentially accelerating flow is composed of two paraboloids at low acceleration, but becomes flattened when the acceleration is high. On the other hand, non-uniqueness occurs for exponentially decelerating flow, when the deceleration exponent has the same value as the zero of the Bessel function.

Two-fluid flow in a tube is an important model for blood flow in micro-vessels of 40-1000 microns, as illustrated by the many examples. Our exact solutions may serve as a base for future more-refined models.

REFERENCES

Bhattacharyya, R.N. (1968). Note on the unsteady flow of two incompressible immiscible fluids between two plates, Bull. Calcutta Math. Soc. Vol.1, pp.129-136.

Bird, R.B., Stewart, W.E., and Lightfoot, E.N. (2007). *Transport Phenomena*, 2nd Ed.,

Wiley, New York.
Bugliarello, G. and Sevilla, J. (1970). Velocity distribution and other characteristics of steady and pulsatile blood flow in fine glass tubes, Biorheology, Vol. 7, pp.85-107.
Chow, J.C.F. (1975). Blood flow: Theory, effective viscosity and effects of particle distribution, Bulletin of Mathematical Biology, Vol. 37, pp. 471-488.
Gaehtgens, P.A.L. (1970). Pulsatile pressure and flow in the mesenteric vascular bed of the cat. Pflugers Archiv Vol. 316, pp. 140-151.
Ghosh, S., Mandal, T.K., Das, G., and Das, P.K. (2009). Review of oil water core annular flow, Ren. Sust. Energy Rev. Vol. 13, pp. 1957-1965.
Hayes, R.H. (1960). Physical basis of the dependence of blood viscosity on tube radius, Am. J. Physiol. Vol. 198, pp.1193-1200.
Intaglietta, M., Richardson, D.A., and Tompkins, W.R. (1971). Blood pressure, flow, and elastic properties in microvessels of cat omentum, Am. J. Physiol. Vol. 221, pp. 922-928.
Kapur, J.N. and Shukla, J.B. (1964). On the unsteady flow of two incompressible immiscible fluids between two plates, Z. Angew. Math. Mech. Vol. 44(6), pp.268-269.
Maarek, J.M.I., Hakim, T.S., and Chang, H.K. (1990). Analysis of pulmonary arterial pressure profile after occlusion of pulsatile blood flow, J. Appl. Physiol. Vol. 68, pp. 761-769.
Martinez-Palou, R., Mosqueira, M.L., Zapata-Rendon, B., Mar-Juarez, E., Bernal-Huicochea, C., Clavel-Lopez, J.C. and Aburto, J. (2011). Transportation of heavy and extra-heavy crude oil by pipeline: A review, Journal of Petroleum Science and Engineering, Vol. 75, pp.274-282.
Pellett, A.A., Johnson, R.W., Morrison, G.G., Champagne, M.S., deBoisblanc, B.P. and Levitzky, M.G. (1999). A comparison of pulmonary arterial occlusion algorithms for estimation of pulmonary capillary pressure. American Journal of Respiratory and Critical Care Medicine Vol. 160, pp. 162-168.
Preziosi, L., Chen, K., and Joseph, D.D. (1989). Lubricated pipelining: stability of core-annular flow, J. Fluid Mech. Vol. 201, pp. 323-356.
Pries, A.R., Secomb, T.W. and Gaehtgens, P. (1996). Biophysics aspects of blood flow in the microvasculature, Cardiovascular Research, Vol. 32, pp. 654-667.
Sanyal, L. (1956). The flow of a viscous liquid in a circular tube under pressure gradients varying exponentially with time, Indian J. Phys. Vol. 30, pp. 57-61.
Secomb, T.W. (1995). Mechanics of blood flow in the microcirculation, in *Biological Fluid Dynamics*, Eds. C.P. Ellington and T.J. Pedley, Society of Experimental Biology, Cambridge, MA pp. 305-321.
Sexl, T. (1930). Uber den von E.G. Richardson entdeckten 'Annulareffekt', Zeit. Phys. Vol. 61, pp. 349-362.
Schlichting, H. and Gersten, K. (2000). *Boundary Layer Theory,* 8th Ed., Springer, Berlin.
Sharan, M. and Popel, A.S. (2001). A two-phase model for flow of blood in narrow tubes with increased effective viscosity near the wall, Biorheology Vol.38, pp.415-428.
Shukla, J.B., Parihar, R.S. and Gupta, S.P. (1980). Effects of peripheral layer viscosity on blood flow through the artery with mild stenosis. Bulletin of Mathematical Biology Vol. 42, pp. 707-805.
Srivastava, V.P. and Saxena, M. (1994). Two-layered model of Casson fluid flow through

stenotic blood vessels, applications to the cardiovascular system. Journal of Biomechanics Vol. 27, pp. 921-928.

Srivastava, L.M. and Srivastava, V.P. (1983). On two-phase model of pulsatile blood flow with entrance effects. Biorheology, Vol. 20, pp. 761-777.

Thomas, C., Bassom, A.P., Blennerhassett, P.J., and Davies, C. (2011). The linear stability of oscillatory Poiseuille flow in channels and pipes, Proc. Roy. Soc. A Vol. 467, pp. 2643-2662.

Vand, V. (1948). Viscosity of solutions and suspensions, I theory, J. Phys. Colloid Chem. Vol. 52, pp.277-299.

Wang, C.Y. (1989). Exact solutions of the unsteady Navier-Stokes equations, Applied Mechanics Reviews, Vol. 42, pp. S269-S282.

Wang, C.Y. (2008). Heat transfer to blood flow in a small tube, J. Fluids Eng. Vol. 130, #024501.

Wang, C.Y. (2017). Starting flow in a channel with two immiscible fluids, Journal of Fluids Engineering, Vol. 139(12), #124501.

Wang, C.Y. and Bassingthwaighte, J.B. (2003). Blood flow in small curved tubes, Journal of Biomechanical Engineering, Vol. 125, pp. 910-913.

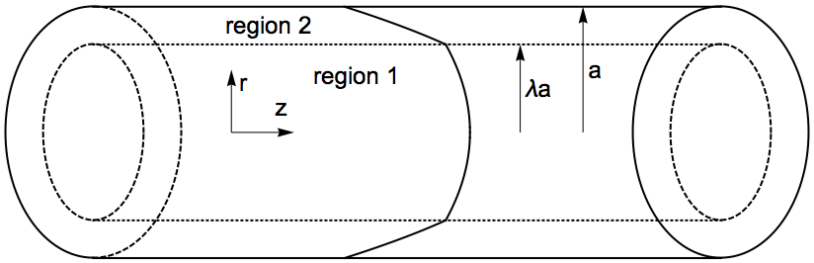

Figure 1. A segment of the tube showing the two regions.

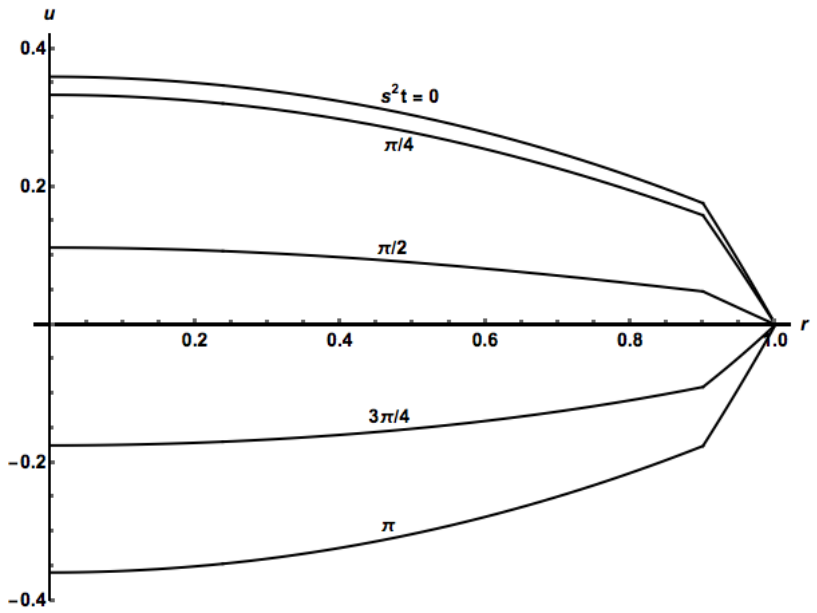

(a)

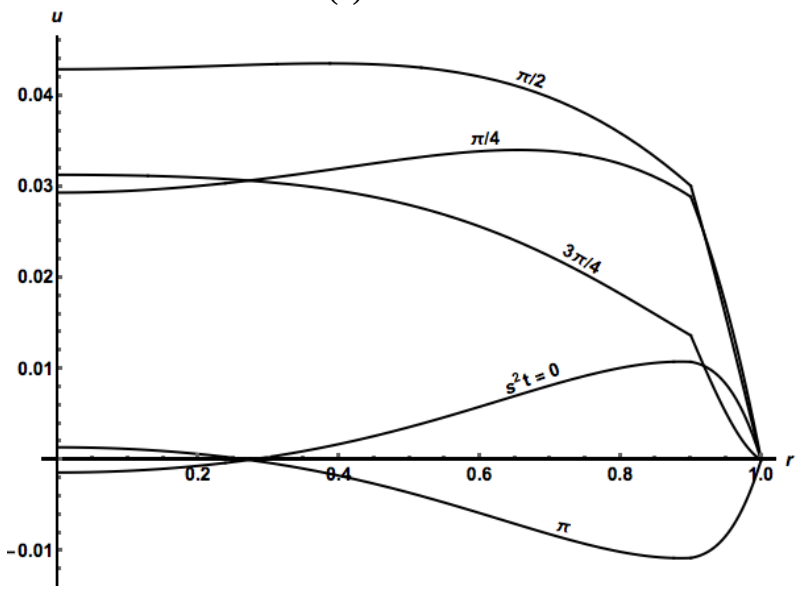

(b)

Figure 2. Velocity profiles for $\gamma = 1$, $\beta = 2$, $\lambda = 0.9$. (a) s=1 (b) s=5

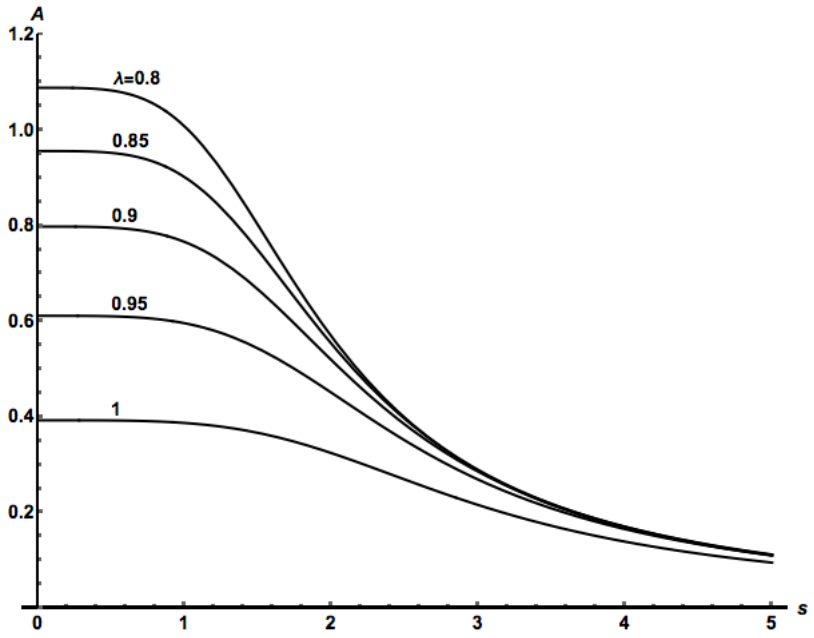

(a)

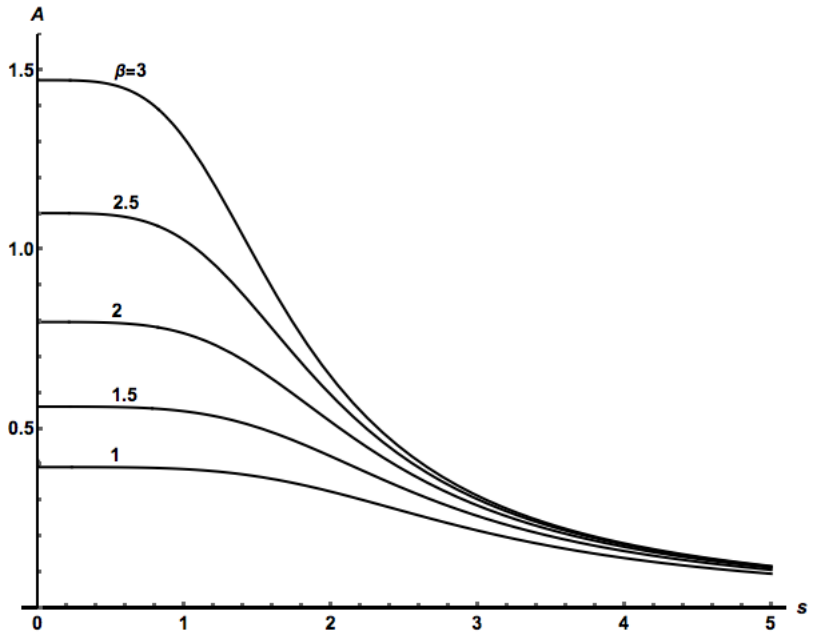

(b)

Figure 3. Flow rate magnitude A as a function of s for $\gamma = 1$ (a) $\beta = 2$ (b) $\lambda = 0.9$

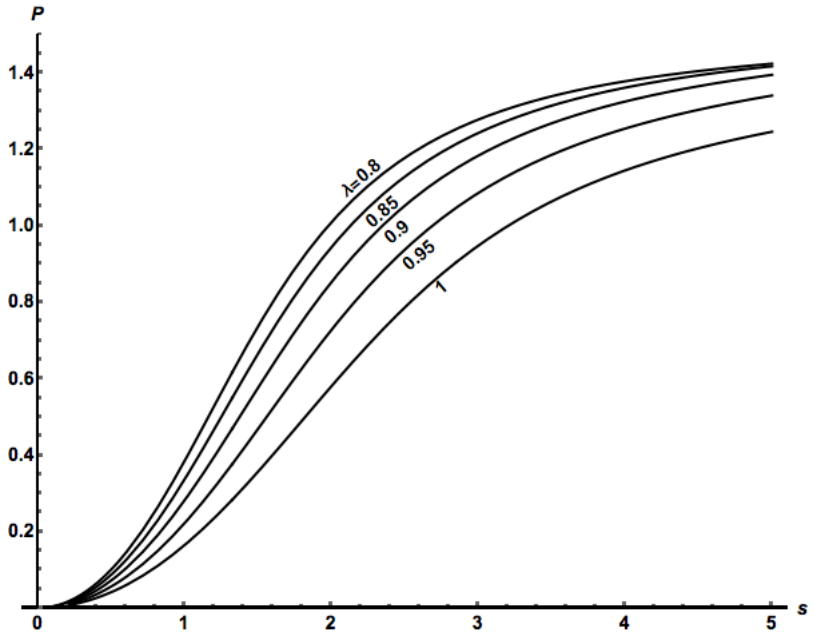

(a)

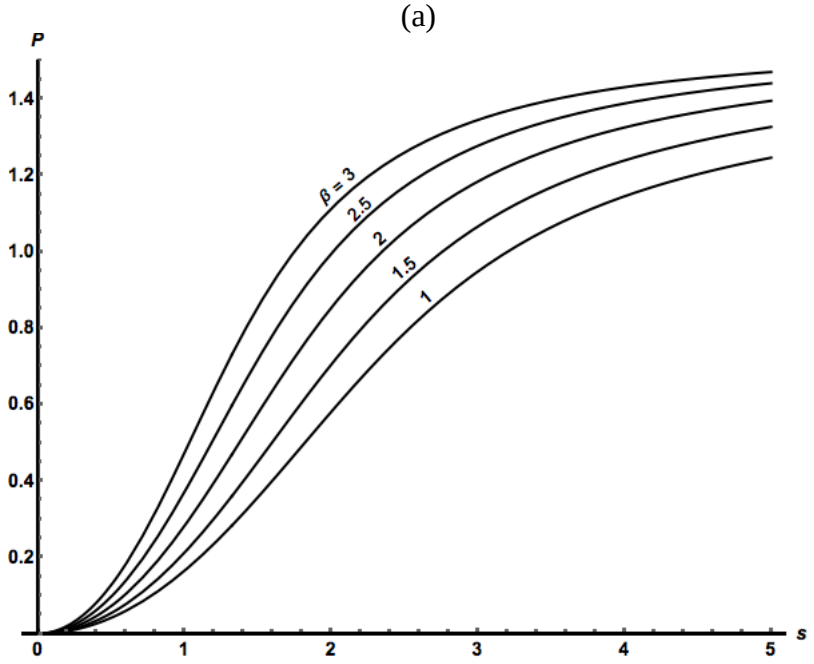

(b)

Figure 4. Flow rate phase lag P as a function of s for $\gamma = 1$ (a) $\beta = 2$ (b) $\lambda = 0.9$

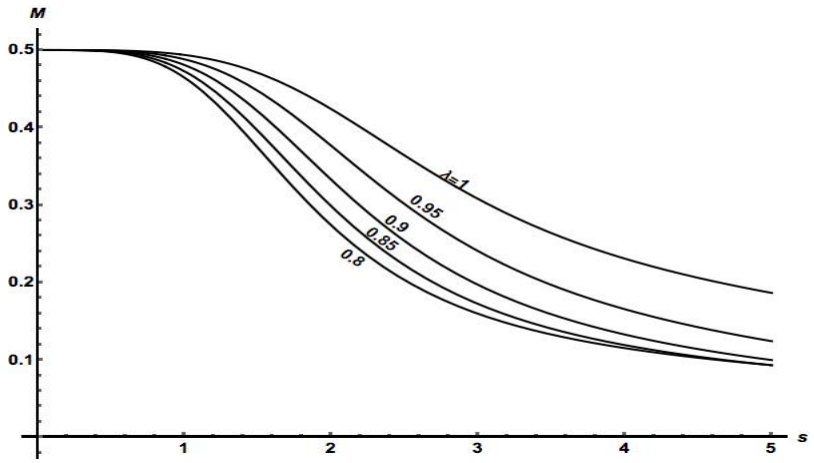

(a)

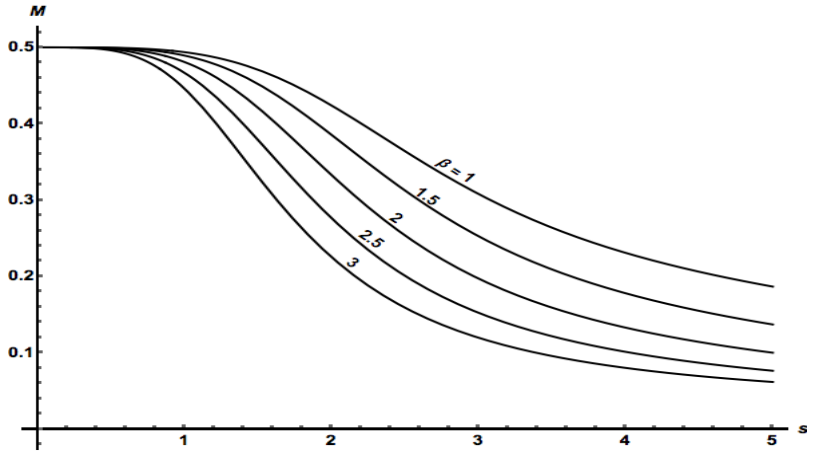

(b)

Figure 5. Shear stress magnitude M as a function of s for $\gamma = 1$ (a) $\beta = 2$ (b) $\lambda = 0.9$

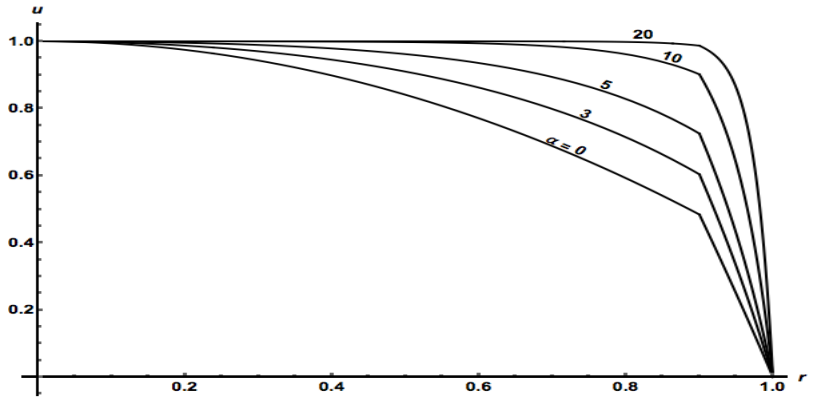

Figure 6. Normalized velocity profiles for exponentially accelerating flow, $\gamma = 1$, $\beta = 2$, $\lambda = 0.9$